Table 1 Input data for numerical example

Parameter and dimensions	Numerical value
Payload mass m_0, slug	6.0
k_1, slug/ft[2a]	0.00087
k_2, slug[b]	0.09
k_3 (dimensionless)[b]	2.0
k_4, ft[4]/slug-sec[2c]	6.9×10^4
k_5, slug	0.03
k_6 (dimensionless)	0.25
k_7 (dimensionless)	2.0
c, fps	7746.

[a] Based on use of type II ribbon chute (Ref. 1, Fig. 22.86, pp. 22–126).
[b] See Ref. 1, Fig. 22.92, pp. 22–130.
[c] For $C_D = 0.5$, $\rho = 0.00238$ slug/ft^3, and $g = 32.2$ ft/sec^2.

are listed in Table 1; v and v_p are left as free variables in the problem.

The results are shown in Fig. 1, in which the ordinate is the ratio of landing system mass to payload mass M/m_0, the abscissa is the ratio of parachute descent velocity to rocket exhaust velocity v_p/c, and each curve is associated with a different value of the ratio of touchdown velocity to rocket exhaust velocity v/c. These results may be used in turn to obtain a plot of M_{opt}/m_0 vs v/c, where M_{opt} is the minimum landing system mass corresponding to the data of Table 1 and to a given v (Fig. 2). Also shown in Fig. 2 is a curve of dimensionless parachute subsystem mass m_r/m_0 vs v/c for a landing system using a parachute subsystem only. (The mass equation for a parachute-only landing system is obtained with the condition that $m_i = m_b = 0$ in the appropriate equations.) That part of Fig. 2 applicable to a parachute-and-retrorocket landing system has been shaded to indicate the portions of landing system mass associated, respectively, with the parachute and retrorocket subsystems. For $v/c < 0.0086$, the parachute-and-retrorocket landing system is lighter.

Variations in M/m_0 resulting from variations in the load factor k_7 can be determined by fixing v/c and calculating a curve of M/m_0 vs v_p/c for each value assumed for k_7. The results of such calculations for a constant value of $v/c = 0$ are shown graphically in Fig. 3.

Discussion

For the example, Figs. 1 and 2 show that the parachute descent velocity associated with M_{opt} and the parachute subsystem portion of M_{opt} remain sensibly constant with respect to variations in v. Thus, the minimum-mass landing system is achieved essentially by letting the parachute subsystem operate at a fixed "optimum" descent velocity and by requiring that the retrorocket subsystem handle any remaining velocity decrement. Figures 2 and 3 show that M_{opt} increases with decreasing touchdown velocity, increases with decreasing load factor, and is insensitive to changes in load factor at relatively high load factors. These results are intuitively evident; however, the figures show the variations quantitatively.

As stated previously, it is desirable to use a high load factor in order to minimize velocity gain due to gravity during the rocket-burning phase of the descent. Also, a high load factor permits use of a relatively short probe if a mechanical probe arrangement is used to sense the altitude for ignition of the retrorocket. However, from an over-all system point of view, one would not use a higher load factor for the rocket phase of the descent than would prevail during other phases of the flight. Also, too high a load factor may, when coupled with subsystem component tolerances, give too little time for effecting release of the chute and ignition of the retrorocket.

For some recovery system designs, parachute weight may depend on conditions at initiation of deployment, rather than on terminal conditions, as was assumed in this analysis. Such a case could be accounted for by use of a heavier type of chute (e.g., Ref. 1, Fig. 22.86, pp. 22–126). In general, however, the weight of a final descent parachute does indeed depend on terminal conditions, since stringent initial conditions may be handled by reefing[3] or by the addition of a small, auxiliary, initial deceleration parachute to the system.

Finally, the analysis of this paper has been conducted with a view to weight optimization only, and other system factors may override weight considerations as such. For example, the relative reliabilities of the parachute-only and the parachute-and-retrorocket landing systems will influence system design.

References

[1] Knacke, T. W., "Recovery systems and equipment," *Handbook of Astronautical Engineering* (McGraw-Hill Book Co., Inc., New York, 1961), pp. 22-123–22-131.

[2] Sutton, G. P., *Rocket Propulsion Elements* (John Wiley and Sons, Inc., New York, 1956), 2nd ed., pp. 17, 380.

[3] "Performance of and design criteria for deployable aerodynamic decelerators," Wright-Patterson Air Force Base Aeronautical Systems Div., ASD-TR-61-579, pp. 183–188 (December 1963).

A High-Vacuum Calibration System

F. G. Sherrell* and A. J. Mathews†
ARO, Inc., Arnold Air Force Station, Tenn.

IONIZATION gages and mass spectrometers must be carefully calibrated before they can be used to indicate total and partial pressures in space simulation chambers. Two possible approaches to this vacuum calibration problem[1] are: 1) a standard vacuum gage might be adopted if one were available (however, the McLeod gage has inadequate accuracy at pressures below 10^{-5} torr, and ionization gages that provide adequate standardization for industrial processing purposes do not satisfy the requirement for calibration against an absolute standard); and 2) absolute, reproducible low pressures can be generated by the multiple-expansion method, the calculated rate-of-rise technique, or one of the various calibrated conductance techniques.[1–3] The vacuum calibration system described here employs a conductance technique using porous molecular leaks in series with a circular orifice.

Technique and System Description

Gas is introduced into the test region (Fig. 1) through a leak of conductance C_1, and the resulting test-region pressure P_2 is calculated by equating the flow through the leak to the flow through the orifice C_2 at equilibrium. Thus

$$C_1(P_1 - P_2) = C_2(P_2 - P_3) \tag{1}$$

In this expression P_1 is the leak forepressure, and P_3 is the

Presented at the AIAA Space Simulation Testing Conference, Pasadena, Calif., November 16–18, 1964 (no preprint number; published in bound volume of preprints of the meeting); revision received March 29, 1965. The research reported in this note was sponsored by the Arnold Engineering Development Center, Air Force Systems Command, under Contract AF 40(600)-1000 with ARO, Inc. Further reproduction is authorized to satisfy needs of the U. S. Government. The authors are pleased to acknowledge the valuable consultations with C. E. Normand of Oak Ridge, Tennessee and C. L. Owens of ARO, Inc.

* Engineering Physicist.
† Electrical Engineer.

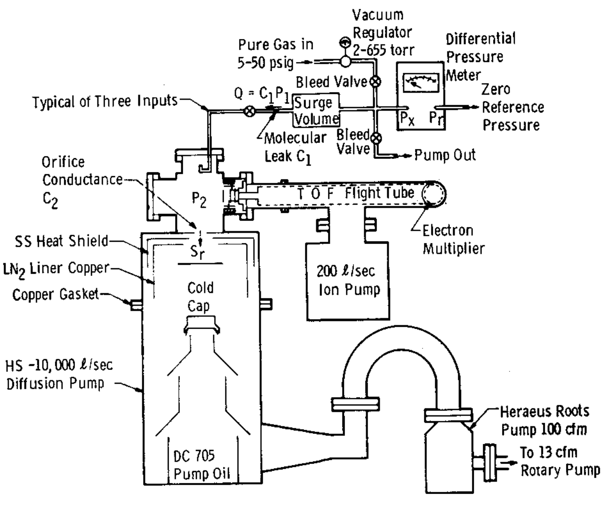

Fig. 1 System schematic.

pressure below the orifice. If we specify $C_1 \ll C_2$, then

$$P_2 = C_1P_1/C_2(1 - P_3/P_2) \tag{2}$$

assuming that no gas is removed from the test region except through the orifice and that the system base pressure is negligible. To apply Eq. (2), we must establish P_3/P_2, which is constant for a given test gas. Normand made this determination for air by taking the ratio of the readings of ionization gages located above and below the orifice.[2] In the present system, direct measurement of P_3/P_2 was avoided, but high accuracy in the calculation of P_2 was retained by providing a very large pumping speed below the orifice as compared to C_2. To clarify, let S_r be the pumping speed from the test region. The flow through the orifice is

$$Q = [P_2\, C_2(1 - P_3/P_2)] = P_2S_r \tag{3}$$

where S_r equals the denominator in Eq. (2); hence,

$$P_2 = C_1P_1/S_r \tag{4}$$

This expression does not include the pressure ratio P_3/P_2, but it requires that S_r be known accurately. Since C_2 and S,

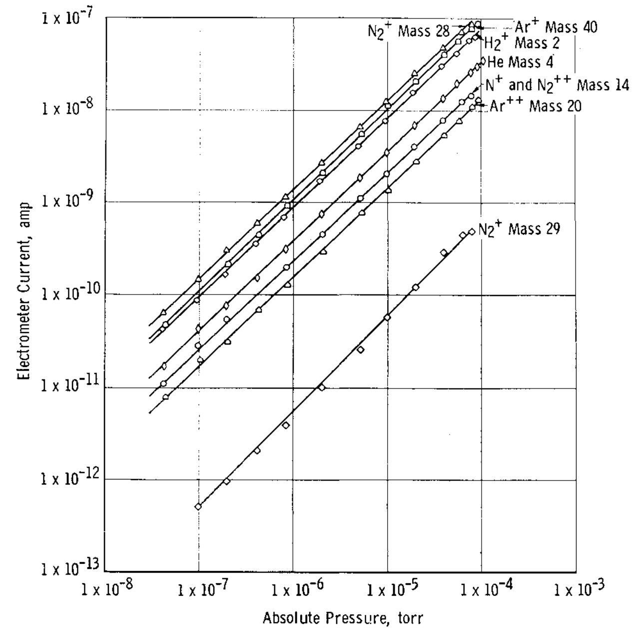

Fig. 2 A partial pressure calibration of the Bendix TOF mass spectrometer (scan channel).

the pumping speed of the cold-trapped diffusion pump, are effectively series conductances, S_r is given by

$$S_r^{-1} = C_2^{-1} + S^{-1} \tag{5}$$

The orifice conductance C_2 is calculated from kinetic theory.[4] High accuracy in the determination of S, discussed later, is not required in the present design because $1/S$ is very small (≈ 0.0004), and its accuracy has little effect on the accuracy of S_r calculated from Eq. (5). After S_r and C_1 have been determined, vacuum calibrations are performed by using Eq. (4) to calculate the test-region pressure.

Figure 1 is a complete schematic of the system. The 8-in.-i.d. $\times$ 9.5-in.-long test region has two 6-in.-diam instrumentation ports on the sides. A Bendix Model 17-210V time-of-flight (TOF) mass spectrometer is shown mounted for calibration. The conductance from the test region to the spectrometer flight tube ($\sim$0.6 l/sec) is negligible as compared to C_2. The pure gases are fed through lines penetrating a third port located at the top of the test region. The 1.008-in.-diam orifice was cut in 0.001-in. stainless-steel sheet after the sheet was welded to a flat ground ring of 5.5 in. o.d. and 4.5 in. i.d. This ring rests in a machined seat at the bottom of the test region. Copper gaskets are used on all of the flanges in the high-vacuum portion of the system. A typical bakeout is 12 hr at 200°C, and system base pressure is about $3 \cdot 10^{-10}$ torr.

Three pure-gas-input systems were provided for establishing known gas mixtures. Equation (4) is applicable to each input independently. This arrangement provides a convenient way to check data-reduction techniques used with mass spectrometers. A typical pure-gas-input system is shown schematically in Fig. 1 and consists of all of the components adjacent to the surge volume. Table 1 gives the details of the three input systems. A detailed discussion of the design and fabrication of the molecular leaks is given in Ref. 5.

Calibration Procedures and Results

The ratio of (C_1/S_r) in Eq. (4) is called the calibration constant, and during system calibration it is the end product sought for each leak using all of the required test gases. The system allows in-place calibration of the three leaks, after the surge volume V of each gas-input system is measured. These volumes are determined by Boyle's law. Results are given in Table 1.

To determine the conductance of a leak, the surge volume is filled with the pure gas, and the gas is allowed to leak out through C_1. An expression relating C_1, P_1, and time is derived readily as

$$V \ln P_1 = -C_1t + V \ln P_{10} \tag{6}$$

where P_{10} is the pressure at $t = 0$. Thus, the value of C_1 is calculated from the slope of the graph of $V \ln P_1$ vs time.

Table 1 Design details of gas-input systems

Feature	Input System		
	No. 1	No. 2	No. 3
Pressure Meter	Model 140 Quartz Gage, Texas Inst.	Type 120 Equibar Transonics	Baratron Mks. Inst.
P_1 Range, torr	1 - 800	0.01 - 30	0.01 - 100
Type of Leak	Porous Vycor Glass	Porous Stainless Steel, Welded In	Porous Stainless Steel, Pressed In
Surge Volume, ℓ	1.24	1.30	1.28

Table 2 Molecular leak conductances, l/sec

Type of Gas	Type of Leak: Porous Vycor	Stainless Steel, Welded Mount	Stainless Steel, Press Mounted
H_2	4.09×10^{-5}	2.67×10^{-4}	3.26×10^{-4}
He	2.95×10^{-5}	1.90×10^{-4}	2.31×10^{-4}
N_2	8.12×10^{-6}	7.27×10^{-5}	8.60×10^{-5}
CO	8.70×10^{-6}	---	8.58×10^{-5}
Ar	7.76×10^{-6}	6.06×10^{-5}	7.23×10^{-5}
CO_2	---	5.69×10^{-5}	---

This technique yields C_1 to within $\pm 2\%$. The molecular leak conductances are given in Table 2.

As shown in Eq. (5), C_2 and S determine the pumping speed from the test region S_r. The orifice conductance for N_2 at 72° F is calculated from the formula of Buneau as follows[4]:

$$C_2 = 3.64A\,(T/M)^{1/2}/\{[(1 - A/A_0)/K] + (3\,L\,A/4\,D_0A_0)\} = 61.5\ l/\text{sec} \quad (7)$$

where A = orifice area (cm²), M = molecular weight, T = absolute temperature, A_0 = test-region area, D_0 = test-region diameter, L = test-region length, and K = 1.002 (from tabulated values).[4]

The determination of S was accomplished by temporarily removing the 1.008-in. orifice and installing a 4.012-in.-diam orifice whose conductance, calculated from Eq. (7), was $C_2' = 1028\ l$/sec. Using an ionization gage calibrated to within an estimated $\pm 10\%$ to read P_2', the measured pumping speed of N_2 through the 4.012-in. orifice was $S_r' = 718 \pm 13\%\ l$/sec. Using these values of C_2' and S_r', S was calculated from Eq. (5) to be $2700 \pm 42\%\ l$/sec. Using this value of S, the pumping speed of N_2 through the 1.008-in. orifice was calculated from Eqs. (7) and (5) to be $S_r = 59.85 \pm 1.1\%\ l$/sec.

A slightly different value could be assigned to S_r for N_2 by taking 59.85 -1.1% l/sec as the low limit, taking the orifice conductance as the upper limit, and writing $S_r = 60.4 \pm 2\%\ l$/sec. The S_r for gas of molecular weight M could then be calculated from the S_r of N_2. Thus

$$S_r = (60.4 \pm 2\%)(28/M)^{1/2} \quad (8)$$

The validity of Eq. (8) follows from Eqs. (5) and (7), after noting that the ratio C_2/S is essentially constant for all of the gases except those cryopumped in the cold trap. For cryopumped gases, S is very large, and S_r is given by $(60.4 + 2\%)\,(28/M)^{1/2}$. Thus, Eq. (8) is valid, even if the test gas is cryopumped. Using the data of Table 2 along with the S_r values calculated from Eq. (8), the calibration constants in Table 3 were calculated. Since C_1 is calibrated to $\pm 2\%$, S_r to $\pm 2\%$, and P_1 is measurable to $\pm 1\%$, the test-region pressure is calculable to $\pm 5\%$.

Table 3 Calibration constants $(C_1/S_r) \times 10^8$

Gas	Input System: No. 1	No. 2	No. 3
H_2	17.4	118	138
He	18.7	119	148
N_2	13.3	123	145
Ar	12.3	118	147

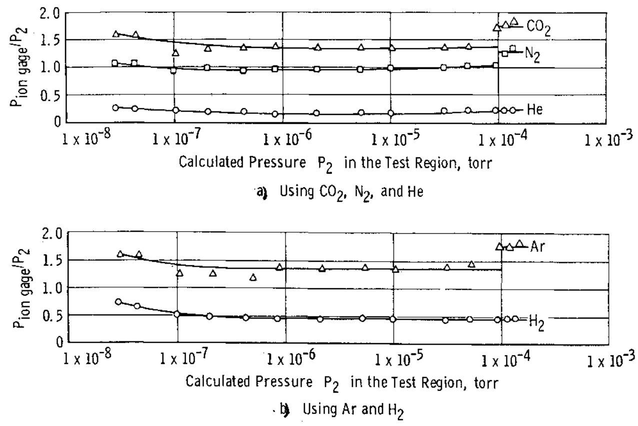

Fig. 3 Calibration of a Veeco RG-75K ionization gage.

System Utilization for Vacuum Calibration

A calibration of one channel of the Bendix 17-210V using H_2, He, N_2, and Ar is shown in Fig. 2. The 17-210V also has been calibrated using CO_2 and O_2. Calibrations of an ionization gage for five gases are shown in Fig. 3. The discontinuities of the Ar, N_2, and CO_2 curves at 10^{-4} torr are attributed, at least partly, to the power supply controlling the emission current at a level 10% too high on the 10^{-4}-torr range. The nonlinearities in the CO_2 and Ar curves in the low 10^{-4-7}-torr range are indications of gage pumping.

Two important considerations affect calibration accuracy: 1) the system should always be pumped to its base pressure prior to calibration and P_2 adjusted upward; and 2) the lowest calibration point of P_2 should be at such a level that the sensor's output is at least 100 times its output at the system base pressure. This will assure that the error caused by the system background is 1% or less. This requirement was not satisfied during the calibrations of Fig. 3, because rigorous bakeout procedures were not followed. Consequently, the gage sensitivity appears to increase in the 10^{-8}-torr range. When these calibrations were made, the system base pressure was about $3 \cdot 10^{-9}$ torr.

Conclusions

The system described generates partial pressures in the 10^{-4} to 10^{-8}-torr range, using the common residual gases except water vapor. The partial pressures produced were calculable to within $\pm 5\%$, and total and partial pressure sensors may be calibrated to this accuracy if the system background pressure is low. Extension of this calibration technique to much lower pressures should be feasible but will depend primarily upon the availability of dependable (UHV) pumping techniques.

References

[1] Florescue, N. A., "Reproducible low pressures and their application to gauge calibration," *Transactions of the Eighth Vacuum Symposium* (Pergamon Press, New York, 1962), pp. 504–510.

[2] Normand, C. E., "Use of a standard orifice in the calibration of vacuum gauges," *Transactions of the Eighth Vacuum Symposium* (Pergamon Press, New York, 1962), pp. 534–543.

[3] Owens, C. L., "Calibration of ionization gages using a porous plug and orifice," Arnold Engineering Development Center TDR-62-139 (August 1962).

[4] Buneau, A. J., Laslett, L. J., and Keller, J. M., "Pumping speed of circular aperturte in diaphragm across circular tube," Rev. Sci. Instr. **23**, 683–686 (1952).

[5] Mathews, A. J., "Evaluation of porous materials as molecular leaks," Arnold Engineering Development Center TDR-64-94 (July 1964).